Entanglement entropy dynamics of non-Gaussian states in free boson systems: Random sampling approach

Ryui Kaneko ⬤,[1,*] Daichi Kagamihara ⬤,[2,†] and Ippei Danshita ⬤[3,‡]

[1]*Physics Division, Sophia University, Chiyoda, Tokyo 102-8554, Japan*
[2]*Department of Physics, Chuo University, Bunkyo, Tokyo 112-8551, Japan*
[3]*Department of Physics, Kindai University, Higashi-Osaka, Osaka 577-8502, Japan*

We develop a random sampling method for calculating the time evolution of the Rényi entanglement entropy after a quantum quench from an insulating state in free boson systems. Because of the non-Gaussian nature of the initial state, calculating the Rényi entanglement entropy calls for the exponential cost of computing a matrix permanent. We numerically demonstrate that a simple random sampling method reduces the computational cost of a permanent; for an $N_s \times N_s$ matrix corresponding to N_s sites at half filling, the sampling cost becomes $O(2^{\alpha N_s})$ with a constant $\alpha \ll 1$, in contrast to the conventional algorithm with the $O(2^{N_s})$ number of summations requiring the exponential time cost. Although the computational cost is still exponential, this improvement allows us to obtain the entanglement entropy dynamics in free boson systems for more than 100 sites. We present several examples of the entanglement entropy dynamics in low-dimensional free boson systems.

I. INTRODUCTION

Understanding the dynamics of quantum many-body systems is a central issue in modern physics. The entanglement entropy is a key quantity that characterizes the dynamics of quantum many-body systems. For example, temporal entanglement entropy can signal quantum phase transitions, helping us identify and understand new phases of matter in nonequilibrium quantum systems [1]. Additionally, it provides insights into how information flows and evolves in quantum systems [2]. Since entanglement is a crucial resource for quantum computing and cryptography, understanding its dynamics may lead to the development of efficient quantum algorithms and secure communication protocols [2,3]. These studies motivate us to investigate the thermalization process in quantum many-body systems and the propagation of quantum information [4–35]. Although the von Neumann entanglement entropy is not a directly measurable quantity, there are several proposals to measure Rényi entanglement entropy [36–38]. Recent experiments have successfully observed the dynamics of the Rényi entanglement entropy using ultracold atoms in optical lattices [39,40] and trapped ions [41].

The numerical simulation of dynamics of the entanglement entropy is also an important approach to understanding quantum many-body systems and providing a benchmark for experiments. Studying the efficiency of numerical simulations provides insights into problems that are challenging in classical systems but can be effectively addressed in quantum systems [42]. In some equilibrium systems, the Rényi entanglement entropy can be efficiently calculated using quantum Monte Carlo simulations [43,44]. This approach allows for accurate entanglement measurements in large and complex systems, shedding light on their universal properties. However, this efficiency in classical simulations does not always extend to nonequilibrium and general equilibrium quantum systems. Finding efficient simulation methods for such systems would guide which problems are most suitable for applying digital and analog quantum simulations.

In contrast to fermion and spin systems, boson systems are much harder to simulate because of the large number of local Hilbert spaces. Even in the free boson systems with simple initial states, such as the Mott insulating state and the charge-density-wave (CDW) state, the entanglement entropy dynamics is difficult to calculate because of the non-Gaussian nature of the initial states. Although the analytical formula for the entanglement entropy is formally obtained by a matrix permanent, its numerical evaluation requires the exponential cost [33]. This situation limits the system size that can be studied to a few tens of sites or particles. Therefore, understanding dynamics of the entanglement entropy in boson systems remains to be a challenging problem even in noninteracting systems.

In this paper, we develop a random sampling method for calculating the time evolution of the Rényi entanglement entropy in free boson systems. In the developed method, we still need to evaluate the matrix permanent, which requires the exponential computational cost in general. However, the growth rate of the computational cost is much slower than the exact permanent calculation. We numerically found that the computational cost is reduced to $O(2^{\alpha N_s})$ with a small constant $\alpha \ll 1$ and the system size N_s. To be more specific, we calculated the size-dependent statistical error of the entanglement entropy, which scales as $\sqrt{c/N_{\text{total}}}$, with c being a size-dependent constant and N_{total} being the total number of

---
*Contact author: ryuikaneko@sophia.ac.jp
†Contact author: dkagamihara119@g.chuo-u.ac.jp
‡Contact author: danshita@phys.kindai.ac.jp

samples, and investigated how c grows with the system size, which represents the number of samples required to achieve a given statistical error. The constant α for the sampling cost is defined by

$$c = 2^{\alpha N_{\mathrm{s}} + \mathrm{const.}}. \tag{1}$$

This improvement enables us to study dynamics of the entanglement entropy in free boson systems for more than 100 sites, confirming that the entanglement entropy in the long-time region exhibits the volume-law scaling as expected.

This paper is organized as follows. In Sec. II, we briefly review the calculation of the Rényi entanglement entropy in free boson systems and describe the conventional algorithm for evaluating the entanglement entropy, which requires the computation of a matrix permanent. To reduce the computational cost, we propose a random sampling method for the matrix permanent. In Sec. III, we examine the performance of the random sampling method by estimating the size dependence of the statistical error. We then present numerical results for dynamics of the entanglement entropy in free boson systems for spatial one (1D) and two dimensions (2D). Finally, in Sec. IV, we summarize our results and discuss future prospects. For simplicity, we set $\hbar = 1$ and take the lattice constant to be unity throughout this paper.

II. RANDOM SAMPLING METHOD FOR ENTANGLEMENT ENTROPY

We first briefly review how to evaluate time evolution of the Rényi entanglement entropy in free boson systems in the case that the initial state is an insulating state. Let us consider dynamics subjected to a quantum quench in the Bose-Hubbard model under the open boundary condition. The Hamiltonian is defined as

$$\hat{H} = -J \sum_{\langle j,l \rangle} (\hat{b}_j^\dagger \hat{b}_l + \mathrm{H.c.}) + \sum_j \Omega_j \hat{n}_j + \frac{U}{2} \sum_j \hat{n}_j (\hat{n}_j - 1), \tag{2}$$

where the symbols $\hat{b}_j$ and $\hat{n}_j$ are the boson annihilation and number operators, respectively. The parameters J, U, and Ω_j represent the strength of the hopping, the strength of the interaction, and the single-particle potential, respectively. The symbol $\langle j, l \rangle$ means that sites j and l are nearest neighbors.

We focus on a sudden quench from an insulating state to the noninteracting ($U = 0$) and homogeneous ($\Omega_j = 0$) point. The following discussion may also be applicable to the case of a quench to the noninteracting and inhomogeneous point; however, we do not consider such a case in this paper for simplicity. The quench to the interacting point is also interesting, but the system becomes nonintegrable and it is beyond the scope of this paper.

As an initial state, we specifically choose the $010101\cdots$-type CDW state at half filling. Although the following formalism also holds for any Fock initial state with any noninteracting Hamiltonian after the quench, we focus on the CDW state for simplicity. It is defined as

$$|\psi\rangle = \prod_{j \in \mathrm{G_{CDW}}} \hat{b}_j^\dagger |0\rangle, \tag{3}$$

where $|0\rangle$ is the vacuum state of $\hat{b}_j$. The $\mathrm{G_{CDW}}$ corresponds to the set of charge rich sites. For example, $\mathrm{G_{CDW}} = \{2, 4, 6, \dots\}$ in 1D, and $\mathrm{G_{CDW}} = \{(2, 1), (4, 1), (6, 1), \dots (1, 2), (3, 2), (5, 2) \dots (2, 3), (4, 3), (6, 3), \dots (1, 4), (3, 4), (5, 4), \dots\}$ in 2D, respectively. Hereafter, in 2D, we map the site index $j(= j_x + L_x j_y)$ one-to-one to the lattice site (j_x, j_y) for $j_x = 1, 2, \dots, L_x$ and $j_y = 1, 2, \dots, L_y$ on a square lattice with L_x (L_y) being the length of the side along the x (y) direction, respectively. The number of sites is represented as N_{s}, which is taken as an even number in our study. Then, the number of particles is $N_{\mathrm{b}} = N_{\mathrm{s}}/2$. The CDW state can be obtained as the ground state of the Bose-Hubbard model at half filling for $\Omega/J \gg 1$ and $U/J \gg 1$ when $\Omega_j = \Omega(-1)^{j+1}$ in 1D and $\Omega_j = \Omega(-1)^{j_x + j_y}$ in 2D, respectively. One can prepare the CDW state in experiments using a secondary optical lattice, which has a lattice constant twice as large as that of the primary lattice [16]. Note that such CDW states and also the Mott insulating state that appear in the Bose-Hubbard model are non-Gaussian states, although the counterparts in the Fermi-Hubbard model are Gaussian states.

To make the discussion self-contained, we summarize the calculation of the Rényi entanglement entropy in free boson systems [33]. We previously evaluated the second Rényi entanglement entropy, which is defined by

$$S_2(t) = -\ln \mathrm{Tr_G}[\hat{\rho}_\mathrm{G}(t)]^2, \tag{4}$$

for the time-evolved state, $|\psi(t)\rangle = \exp(-i\hat{H}t)|\psi\rangle$ [33]. Here, $\hat{\rho}_\mathrm{G}(t)$ is the reduced density matrix and $\mathrm{Tr_G}$ is the trace over the basis of subsystem G that contains $l = 1, 2, \dots, N_\mathrm{G}$ sites. For simplicity, we set N_G to half the system size ($N_\mathrm{G} = N_{\mathrm{s}}/2$) throughout this paper. The reduced density matrix $\hat{\rho}_\mathrm{G}(t)$ and the product of two copies of the state $|\psi(t)\rangle$, i.e., $|\psi_{\mathrm{copy}}(t)\rangle := |\psi(t)\rangle \otimes |\psi(t)\rangle$, are related as

$$\mathrm{Tr_G}[\hat{\rho}_\mathrm{G}(t)]^2 = \langle \psi_{\mathrm{copy}}(t)|\hat{V}_\mathrm{G}|\psi_{\mathrm{copy}}(t)\rangle, \tag{5}$$

with $\hat{V}_\mathrm{G}(t)$ being the shift operator that swaps states in subsystem G. Therefore, we need to evaluate the right-hand side of the above equation by explicitly calculating the time-evolved state $|\psi(t)\rangle$. For any noninteracting Hamiltonian $\hat{H}_0$, by diagonalizing it in the first-quantization representation, we can express it as

$$\hat{H}_0 = -J \sum_{\langle j,l \rangle} (\hat{b}_j^\dagger \hat{b}_l + \mathrm{H.c.}) = \sum_{k=1}^{N_{\mathrm{s}}} \epsilon_k \hat{\beta}_k^\dagger \hat{\beta}_k, \quad \hat{\beta}_k = \sum_{j=1}^{N_{\mathrm{s}}} x_{k,j} \hat{b}_j, \tag{6}$$

where $\hat{b}_j$ is the annihilation operator in the original basis of the Hamiltonian and $\hat{\beta}_k$ is the annihilation operator in the basis diagonalizing the Hamiltonian. The kth eigenenergy of $\hat{H}_0$ is represented as ϵ_k and the corresponding eigenvector is expressed as $\boldsymbol{x}_k$. The elements of the eigenvector $\boldsymbol{x}_k$ are real numbers when the hopping strength J is real. Straightforward calculations for $\hat{H} = \hat{H}_0$ lead to the expression of the

time-evolved state as

$$|\psi(t)\rangle = \exp(-i\hat{H}_0 t) \prod_{j \in G_{CDW}} \hat{b}_j^\dagger |0\rangle \tag{7}$$

$$= \prod_{j \in G_{CDW}} [\exp(-i\hat{H}_0 t) \hat{b}_j^\dagger \exp(i\hat{H}_0 t)]|0\rangle \tag{8}$$

$$= \prod_{j \in G_{CDW}} \left\{ \sum_{j'=1}^{N_s} \left[\sum_{k=1}^{N_s} x_{k,j} x_{k,j'} \exp(-i\epsilon_k t) \right] \hat{b}_{j'}^\dagger \right\} |0\rangle. \tag{9}$$

Here, we use the fact that $\exp(\pm i\hat{H}_0 t)|0\rangle = |0\rangle$. For convenience, we define the correlation $y_{i,j}(t)$ ($i, j = 1, 2, \ldots, N_s$) as

$$y_{i,j}(t) = \sum_{k=1}^{N_s} x_{k,i} x_{k,j} \exp(-i\epsilon_k t). \tag{10}$$

Then, the time-evolved state is expressed as

$$|\psi(t)\rangle = \prod_{j \in G_{CDW}} \left\{ \sum_{j'=1}^{N_s} y_{j,j'}(t) \hat{b}_{j'}^\dagger \right\} |0\rangle. \tag{11}$$

The state $|\psi_{copy}(t)\rangle$ is obtained as a tensor product of two $|\psi(t)\rangle$ states. Because both $|\psi_{copy}(t)\rangle$ and $\hat{V}_G|\psi_{copy}(t)\rangle$ are many-boson states and their wave functions are symmetric under the exchange of bosons, the expectation value of the shift operator $\langle\psi_{copy}(t)|\hat{V}_G|\psi_{copy}(t)\rangle$ is given by the permanent of a certain matrix consisting of single-particle correlation functions, defined by

$$z_{i,j}(t) = \sum_{l \in G} y_{r_i,l}^*(t) y_{r_j,l}(t), \tag{12}$$

with r_i and r_j being indices of charge rich sites ($r_i, r_j \in G_{CDW}$). Consequently, using the matrix Z with elements $z_{i,j}(t)$, we can express the Rényi entanglement entropy at time t as

$$S_2 = -\ln \text{perm}A, \tag{13}$$

$$A = \begin{pmatrix} Z & I - Z \\ I - Z & Z \end{pmatrix}. \tag{14}$$

Here, perm$A$ is the matrix permanent, which is defined as the sum of all the products of the elements of the matrix A, given as

$$\text{perm}A = \sum_{f \in \mathfrak{S}_{N_s}} \prod_{j=1}^{N_s} a_{j,f(j)}, \tag{15}$$

with $\mathfrak{S}_{N_s}$ being the set of all permutations. Then, A is an $N_s \times N_s$ square matrix, I is an $N_s/2 \times N_s/2$ identity matrix, and Z is an $N_s/2 \times N_s/2$ matrix with elements $z_{i,j}(t)$.

Note that the matrix Z takes the form in Eq. (12) for any initial Fock state and any quadratic Hamiltonian [33]. In this paper, we focus on the CDW initial state and the free boson Hamiltonian with the nearest-neighbor hopping on a chain and a square lattice. In 1D, the matrix representation of $\hat{H}_0$ in the basis of $\hat{b}_j$ is given by

$$h_{0,j,l} = \begin{cases} -J & (|j-l|=1), \\ 0 & (\text{otherwise}), \end{cases} \tag{16}$$

which is an $N_s \times N_s$ tridiagonal matrix. The eigenvalues and eigenvectors are easily obtained as

$$\epsilon_k = -2J \cos\left(\frac{k\pi}{N_s+1}\right), \tag{17}$$

$$x_{k,l} = \sqrt{\frac{2}{N_s+1}} \sin\left(\frac{k\pi}{N_s+1} l\right), \tag{18}$$

where $k, l = 1, 2, \ldots, N_s$. In 2D, the matrix representation of $\hat{H}_0$ in the basis of $\hat{b}_j$ is given by

$$h_{0,j,l} = \begin{cases} -J & (\sqrt{(j_x-l_x)^2+(j_y-l_y)^2}=1), \\ 0 & (\text{otherwise}), \end{cases} \tag{19}$$

where $j = j_x + L_x j_y$ and $l = l_x + L_x l_y$. This $N_s \times N_s$ matrix is no longer tridiagonal. We numerically diagonalize the matrix h_0 to obtain the eigenvalues ϵ_k and eigenvectors x_k.

In general, the calculation of the matrix permanent in Eq. (13) requires the exponential cost of $O(N_s \times 2^{N_s})$ for an $N_s \times N_s$ matrix. The well-known algorithms for evaluating matrix permanents are the Ryser formula [45–47] and Balasubramanian-Bax-Franklin-Glynn (BBFG) formula [47–51]. For example, in the BBFG algorithm, the permanent for an $n \times n$ matrix (A) is evaluated as

$$\text{perm}A = \frac{1}{2^{n-1}} \sum_{\delta} \left(\prod_{k=1}^n \delta_k\right) \prod_{j=1}^n \sum_{i=1}^n \delta_i a_{ij}. \tag{20}$$

Here, a_{ij} is the element of the matrix A, and the summation is taken over $\delta = (\delta_1, \delta_2, \ldots, \delta_n) \in \{\pm 1\}^n$ with $\delta_1 = 1$. The exponential time cost stems from the fact that the number of terms in the summation grows exponentially in n.

To evaluate the permanent of an $n \times n$ matrix A more efficiently, we propose a random sampling method. Instead of taking all the terms in the summation in Eq. (20), we randomly sample a subset of terms. We replace the sum over the vector δ in Eq. (20) by the random vector r. Note that the equivalent sampling procedure itself is proposed in Ref. [52], although the context is different and the efficiency of the random sampling that we adopt here is not discussed. As we show below, this method allows us to approximately evaluate the permanent with the matrix size larger than 100, which is difficult to achieve with the conventional Ryser and BBFG algorithms.

To simplify the notation, let us introduce the Glynn estimator for an $n \times n$ complex matrix A and the complex vector x [47,53–55], which is defined as

$$\text{Gly}_x(A) = \prod_{k=1}^n x_k^* \prod_{i=1}^n \left(\sum_{j=1}^n a_{ij} x_j\right). \tag{21}$$

When we specifically choose a random variable r, which has elements $r_i \in \mathbb{C}$ ($i = 1, 2, \ldots, n$) that are independently chosen uniformly on $|r_i| = 1$, we can evaluate the permanent of the matrix as the expectation value of the Glynn estimator $\text{Gly}_r(A)$ [47,53–55]. The relation is given as

$$\text{perm}A = \mathbb{E}[\text{Gly}_r(A)] = \mathbb{E}\left[\prod_{i=1}^n r_i^* \left(\sum_{j=1}^n a_{ij} r_j\right)\right], \tag{22}$$

where $\mathbb{E}$ means the expectation value. This equation can be shown by expanding the product

$$\mathbb{E}[\mathrm{Gly}_{\boldsymbol{r}}(A)] = \mathbb{E}\left[\prod_{i=1}^{n} r_i^*(a_{i1}r_1 + a_{i2}r_2 + \cdots + a_{in}r_n)\right] \quad (23)$$

$$= \mathbb{E}\left[(r_1^* r_2^* \cdots r_n^*)\prod_{i=1}^{n}(a_{i1}r_1 + a_{i2}r_2 + \cdots + a_{in}r_n)\right] \quad (24)$$

$$= \mathbb{E}\left[(r_1^* r_2^* \cdots r_n^*)\right.$$
$$\times \sum_{g(1),g(2),\ldots,g(n)\in\{1,2,\ldots,n\}} a_{1g(1)}a_{2g(2)}\cdots a_{ng(n)}$$
$$\left. \times (r_{g(1)}r_{g(2)}\cdots r_{g(n)})\right] \quad (25)$$

$$= \sum_{g(1),g(2),\ldots,g(n)\in\{1,2,\ldots,n\}} a_{1g(1)}a_{2g(2)}\cdots a_{ng(n)}$$
$$\times \mathbb{E}[(r_1^* r_2^* \cdots r_n^*)(r_{g(1)}r_{g(2)}\cdots r_{g(n)})]. \quad (26)$$

If the map $i \mapsto g(i)$ is a permutation, one can always find a unique pairing between r_i^* and $r_{g(j)}$ for all $i[= g(j)]$ and j, and the expectation value satisfies

$$\mathbb{E}[(r_1^* r_2^* \cdots r_n^*)(r_{g(1)}r_{g(2)}\cdots r_{g(n)})]$$
$$= \mathbb{E}[|r_1|^2 |r_2|^2 \cdots |r_n|^2] = \mathbb{E}[1^n] = 1; \quad (27)$$

otherwise it is zero because there exists at least one unpaired and independent r_i^* that satisfies $\mathbb{E}[r_i^*] = 0$. Then, we obtain

$$\mathbb{E}[\mathrm{Gly}_{\boldsymbol{r}}(A)] = \sum_{g(1),g(2),\ldots,g(n)\in\mathfrak{S}_n} a_{1g(1)}a_{2g(2)}\cdots a_{ng(n)}, \quad (28)$$

which gives the permanent of the matrix A in Eq. (15). Therefore, we can calculate the permanent by the following sample mean:

$$\mathrm{perm}A \approx \frac{1}{N_{\mathrm{smp}}}\sum_{m=1}^{N_{\mathrm{smp}}} p^{(m)}, \quad (29)$$

$$p^{(m)} = \prod_{i=1}^{n} r_i^{(m)*}\left(\sum_{j=1}^{n} a_{ij}r_j^{(m)}\right), \quad (30)$$

where N_{smp} is the number of samples and $\boldsymbol{r}^{(m)}$ is a complex random vector of a sample m. In practice, we take $r_i^{(m)} = \exp[i\theta_i^{(m)}]$ with $\theta_i^{(m)}$ chosen uniformly in $[0, 2\pi)$ [54–56]. The value $p^{(m)}$ is a complex number for each sample m.

In the present system with $n = N_{\mathrm{s}}$, the entanglement entropy satisfies $0 \leqslant S_2 \leqslant cN_{\mathrm{s}}$ with c being a sufficiently large constant, and therefore, the condition $\exp(-cN_{\mathrm{s}}) \leqslant \mathrm{perm}A \leqslant 1$ holds. Since $\mathrm{Re}\, p^{(m)}$ and $\mathrm{Im}\, p^{(m)}$ can be exponentially small in N_{s} and can be both positive and negative, we need $N_{\mathrm{smp}} = O[\exp(\alpha N_{\mathrm{s}})]$ samples with a constant α to accurately estimate $\mathrm{perm}A$ in general. The situation is similar to the case of systems having the notorious negative sign problems [57]. The advantage of the present approach is that the constant prefactor α would be sufficiently smaller than
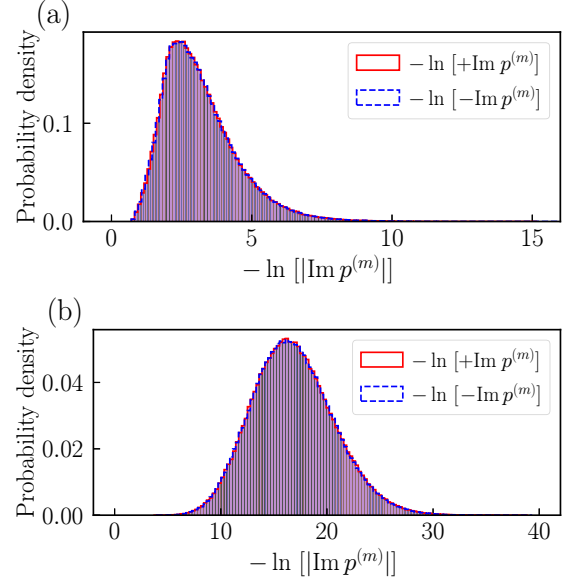

FIG. 1. Distribution of the value $-\ln[|\mathrm{Im}\, p^{(m)}|]$ in Eq. (30). We show the distribution $P(x)$ of $x = -\ln[+\mathrm{Im}\, p^{(m)}]$ ($x = -\ln[-\mathrm{Im}\, p^{(m)}]$) when $\mathrm{Im}\, p^{(m)} > 0$ ($\mathrm{Im}\, p^{(m)} < 0$) with a red solid line (a blue dashed line). (a) At time $tJ = 1$ for $N_{\mathrm{s}} = 40$. (b) At time $tJ = 2N_{\mathrm{s}}$ for $N_{\mathrm{s}} = 40$. In both cases, the positive and negative components exhibit nearly the same distribution, suggesting that $\mathrm{perm}A$ does not contain an imaginary part.

unity as far as we deal with the matrix A generated in the present system [see Eq. (14)]. Indeed, we numerically found that $\alpha \approx 0.2$. One may also consider the importance sampling to reduce the variance of the estimator in Eq. (21). However, we do not use it in the present study and stick to the simple random sampling method because we are interested in how far we can go with the primitive procedure. Note that, although we here focus on the CDW initial state to be specific, the approach described above is applicable also to other insulating initial states as long as they are expressed as a simple product of local Fock states.

III. RESULTS

Hereafter, we present the numerical results on dynamics of the entanglement entropy in hypercubic lattices, such as a chain in 1D and a square lattice in 2D. The number of sites is given by N_{s} on a one-dimensional chain and $N_{\mathrm{s}} = L_x \times L_y$ on a two-dimensional square lattice.

A. Estimation of the statistical error

Before estimating the expectation value and the statistical error of $\mathrm{perm}A$ in Eq. (29), we examine the distribution of the value $p^{(m)}$. For simplicity, we will focus on the one-dimensional case for the moment. We specifically consider the system size $N_{\mathrm{s}} = 40$ and investigate the distribution of 2^{20} samples at a short time ($tJ = 1$) and at a long time ($tJ = 2N_{\mathrm{s}}$).

Let us first look into the imaginary part of each sample required for calculating $\mathrm{Im}\,\mathrm{perm}A$. In the present study, we expect $\mathrm{Im}\,\mathrm{perm}A = 0$ because $\mathrm{perm}A = \exp(-S_2)$ ($S_2 \in \mathbb{R}$) should be real. As shown in Fig. 1, we examine the distribution of the positive and negative $\mathrm{Im}\, p^{(m)}$ at a short time
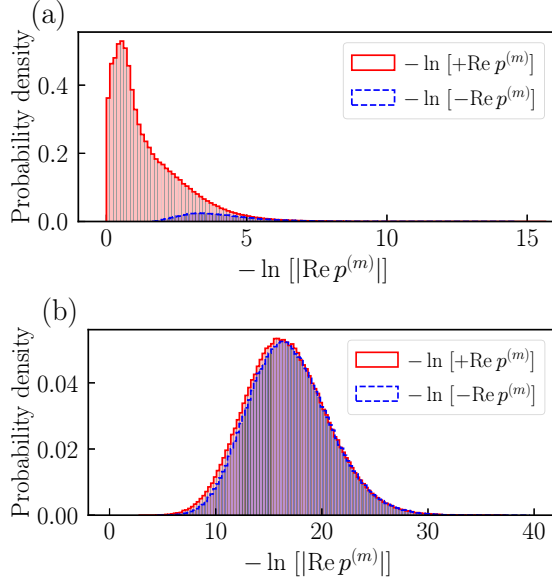
FIG. 2. Distribution of the value $-\ln[|\text{Re}\,p^{(m)}|]$ in Eq. (30). We show the distribution $P(x)$ of $x = -\ln[+\text{Re}\,p^{(m)}]$ ($x = -\ln[-\text{Re}\,p^{(m)}]$) when $\text{Re}\,p^{(m)} > 0$ ($\text{Re}\,p^{(m)} < 0$) with a red solid line (a blue dashed line). (a) At time $tJ = 1$ for $N_s = 40$. Since the positive component is dominant, we expect $\text{perm}A = O(1)$, and thus, $S_2 = O(1)$. (b) At time $tJ = 2N_s$ corresponding to $S_2 = O(N_s)$ for $N_s = 40$. Since the positive and negative components are comparable while the positive one is slightly dominant, we expect $\text{perm}A = O[\exp(-\text{const.} \times N_s)]$, and thus, $S_2 = O(N_s)$.

$tJ = 1$ and at a long time $tJ = 2N_s$. In each time, the positive and negative components exhibit nearly the same shape and cancel each other out, suggesting that $\text{Im}\,\text{perm}A = 0$ as expected when the number of samples is sufficiently large. Indeed, we numerically confirmed that the expectation value of $\text{Im}\,\text{perm}A$ is always zero within the sufficiently small statistical error.

We then investigate the real part of $\text{perm}A$. As in the case of imaginary part, we examine the distribution of the positive and negative $\text{Re}\,p^{(m)}$ at a short time $tJ = 1$ and at a long time $tJ = 2N_s$.

In the short time case ($tJ = 1$), we expect $S_2 = O(1)$ because the entanglement entropy does not grow significantly. Therefore, the condition $\text{perm}A = O(1)$ likely holds. As we expected, the distribution of the positive $\text{Re}\,p^{(m)}$ has much greater weight than the negative one [see Fig. 2(a)]. The positive component has a peak at $\text{Re}\,p^{(m)} \approx +e^{-1}$, whereas the negative component has a peak at $\text{Re}\,p^{(m)} \approx -e^{-3}$. Since the distribution is not a normal distribution, we need careful analysis to estimate the statistical error, as we will show later in this section.

However, in the long time case ($tJ = 2N_s$), we expect $S_2 = O(N_s)$ since the time-evolved state converges to a highly entangled steady state. Therefore, the condition $\text{perm}A = O[\exp(-\text{const.} \times N_s)]$ likely holds, and the sampling must be much harder than the short time case. Indeed, as shown in Fig. 2(b), the positive and negative distributions exhibit a similar shape, indicating that the expectation value is extremely small. At the same time, the area of the positive distribution

is slightly larger than that of the negative one, suggesting that $\text{Re}\,\text{perm}A > 0$. As in the case of a short time, the distribution of $\text{Re}\,p^{(m)}$ is not a normal distribution, which can be confirmed by the presence of two peaks at $\text{Re}\,p^{(m)} \approx \pm e^{-16}$. Therefore, also for the long time case, careful analysis is required to estimate the statistical error.

To estimate the statistical error, we combine the blocking analysis and the bootstrap method. In the blocking analysis, we divide the N_{total} samples in to the N_{block} blocks containing $N_{\text{blocksize}} = N_{\text{total}}/N_{\text{block}}$ samples. For each block j ($= 1, 2, \ldots, N_{\text{block}}$), we calculate the average $p^{(j, N_{\text{blocksize}})}$ of $N_{\text{blocksize}}$ samples. This procedure results in

$$\frac{1}{N_{\text{total}}} \sum_{m=1}^{N_{\text{total}}} p^{(m)} = \frac{1}{N_{\text{block}}} \sum_{j=1}^{N_{\text{block}}} p^{(j, N_{\text{blocksize}})}, \tag{31}$$

$$p^{(j, N_{\text{blocksize}})} = \frac{1}{N_{\text{blocksize}}} \sum_{k=(j-1)N_{\text{blocksize}}+1}^{jN_{\text{blocksize}}} p^{(k)}. \tag{32}$$

We then prepare resampled data by the bootstrap method. To this end, we randomly choose N_{block} samples $q^{(j)}$ ($j = 1, 2, \ldots, N_{\text{block}}$) from the original N_{block} samples $p^{(j, N_{\text{blocksize}})}$ ($j = 1, 2, \ldots, N_{\text{block}}$). Here, we do not avoid picking the same samples multiple times. We repeat this process N_{boot} times and generate samples $\bar{q}^{(k)}$ ($k = 1, 2, \ldots, N_{\text{boot}}$) by calculating

$$\bar{q}^{(k)} = \frac{1}{N_{\text{block}}} \sum_{j=1}^{N_{\text{block}}} q^{(j)} \tag{33}$$

for each k. The number N_{boot} is chosen to be sufficiently large so that the resampled data follows a normal distribution. We estimate the average and the standard error of the samples $\bar{q}^{(k)}$, which gives $\text{perm}A$ and its statistical error $\sigma_{\text{perm}A}$. Then, the statistical error of the Rényi entanglement entropy is evaluated by $\sigma_{S_2} = |-\ln(\text{perm}A + \sigma_{\text{perm}A}) - [-\ln(\text{perm}A)]| \approx |\sigma_{\text{perm}A}/\text{perm}A|$ for $|\sigma_{\text{perm}A}| \ll 1$.

In general, we do not need the blocking analysis; however, the computational cost of the bootstrap method will be extremely high when we directly use the exponentially large number of N_{total} samples. By taking a small constant N_{block}, we can reduce the computational cost of the bootstrap method. Hereafter, we typically choose $N_{\text{block}} = 2^{10}$ and $N_{\text{boot}} = 2^{12}$ and consider exponentially large $N_{\text{total}} \approx \exp(\text{const.} \times N_s)$. Note that the period of the pseudorandom number generator should be sufficiently longer than the number of samples. These parameters allow us to safely obtain a normal distribution of the resampled data (for example, see Fig. 3).

B. Size dependence of the statistical error

To estimate the ideal number of samples that we need for each system size, we examine the size dependence of the number of samples under the fixed statistical error. Here, we focus on the one-dimensional system again. For system sizes $N_s = 16, 20, \ldots, 60$, we increase the number of samples N_{total} up to 2^{30} and calculate the standard error of the Rényi entanglement entropy density, σ_{S_2/N_s}. The standard error for each system size N_s decreases as

$$\sigma_{S_2/N_s} = \sqrt{\frac{c_{1D}(N_s)}{N_{\text{total}}}}, \tag{34}$$
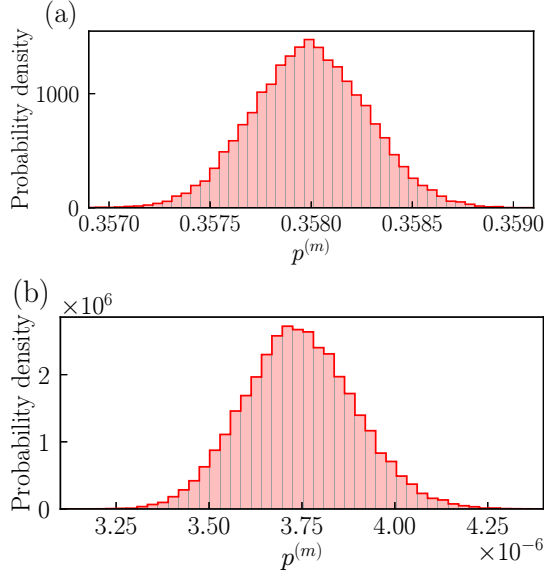
FIG. 3. Estimate of the statistical error using the blocking analysis and the bootstrap method. (a) At time $tJ = 1$ for $N_s = 40$. (b) At time $tJ = 2N_s$ for $N_s = 40$. We choose $N_{total} = 2^{20}$, $N_{block} = 2^{10}$, and $N_{boot} = 2^{12}$. In both cases, the resampled data exhibit a normal distribution, which allows us to estimate the statistical error safely.

with increasing N_{total}, where $c_{1D}(N_s)$ is a constant that depends on N_s [see Fig. 4(a)]. The value $c_{1D}(N_s)$ increases exponentially large with increasing system size N_s in general. By fitting numerical data points, we find

$$c_{1D}(N_s) = 2^{\alpha_{1D} N_s - \beta_{1D}}, \tag{35}$$

$$\alpha_{1D} = 0.219(6), \tag{36}$$

$$\beta_{1D} = 8.8(3), \tag{37}$$

as shown in Fig. 4(b). This result suggests that the number of samples should be

$$N_{total} = \frac{c_{1D}(N_s)}{(\sigma_{S_2/N_s})^2} \approx \frac{2^{0.2 \times N_s - 9}}{(\sigma_{S_2/N_s})^2} \tag{38}$$

to keep the statistical error σ_{S_2/N_s} constant. When we wish to suppress the statistical error, e.g., $\sigma_{S_2/N_s} = 2^{-10}$, the number of samples should be larger than $N_{total} = 2^{0.2 N_s + 11}$.

The computational cost is proportional to the number of samples and is $O(2^{\alpha_{1D} N_s})$ with $\alpha_{1D} \approx 0.2 \ll 1$ in the one-dimensional case. Consequently, the random sampling method is much more efficient than the conventional algorithms in Eq. (20), requiring the summation of 2^{N_s} terms.

The similar small constant prefactor $\alpha_{2D} \approx 0.2$ is also found in the two-dimensional case by analyzing systems up to 120 sites. As shown in Fig. 5(a), we extract the size dependence of the coefficient $c_{2D}(N_s)$ in the fitting function

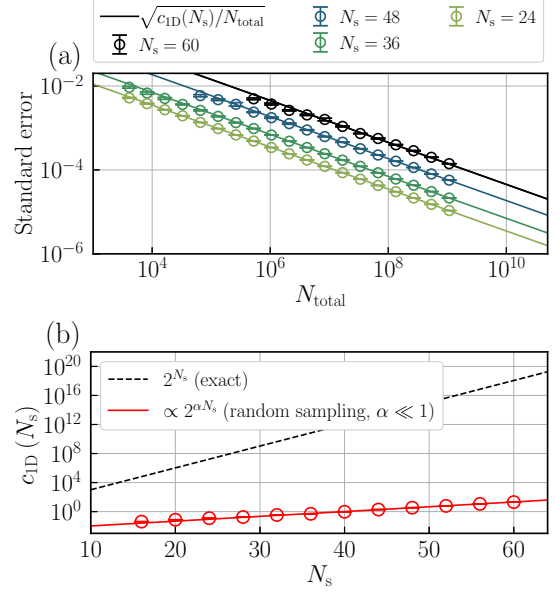$$\sigma_{S_2/N_s} = \sqrt{\frac{c_{2D}(N_s)}{N_{total}}}. \tag{39}$$

FIG. 4. (a) Size dependence of the standard error of Rényi entanglement entropy density σ_{S_2/N_s} at time $tJ = 2N_s$ as a function of the number of total samples N_{total} in 1D. The statistical error is estimated by the blocking analysis and the bootstrap method with $N_{block} = 2^{10}$ and $N_{boot} = 2^{12}$. The error bar of σ_{S_2/N_s} is estimated for 32 independent simulations. The statistical error should satisfy $\sigma_{S_2/N_s} = \sqrt{c_{1D}(N_s)/N_{total}}$ with $c_{1D}(N_s)$ being a size-dependent constant. (b) Constant $c_{1D}(N_s)$ as a function of size N_s. The value $c_{1D}(N_s)$ represents the number of samples required to achieve a given statistical error σ_{S_2/N_s}. We find that it satisfies $c_{1D}(N_s) \approx 2^{0.2 N_s - 9}$ by fitting data for $N_s \geqslant 40$. It is much smaller than the number of terms (2^{N_s}) in the summation in Eq. (20), suggesting that the computational cost is moderate although it is exponential in N_s.

We find that the value $c_{2D}(N_s)$ satisfies

$$c_{2D}(N_s) = 2^{\alpha_{2D} N_s - \beta_{2D}}, \tag{40}$$

$$\alpha_{2D} = 0.20(8), \tag{41}$$

$$\beta_{2D} = 13(4), \tag{42}$$

as shown in Fig. 5(b). Therefore, the computational cost is also $O(2^{\alpha_{2D} N_s})$ with $\alpha_{2D} \approx 0.2 \ll 1$ in the two-dimensional case. In practice, as for the system size $N_s = 10 \times 10$ at the time point $tJ = 20$, it takes less than a day to calculate the Rényi entanglement entropy using a single core central processing unit.

C. Entanglement entropy dynamics

By taking advantage of the random sampling method, we calculate the dynamics of Rényi entanglement entropy density after a sudden quench. Hereafter, we choose the number of samples $N_{total} = 2^{0.2 N_s + 12}$ to keep the statistical error sufficiently small.

Let us first compare our present result with the exact one calculated with the largest size $N_s = 40$ in our previous study [33] in the case of 1D. As shown in Fig. 6(a), the random sampling method provides the exact Rényi entanglement entropy density within the statistical error bar.
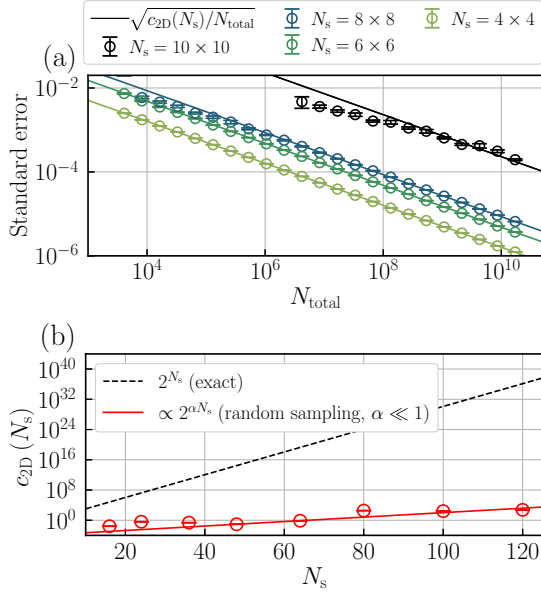
FIG. 5. (a) Size dependence of the standard error of Rényi entanglement entropy density σ_{S_2/N_s} at time $tJ = 2L_x$ as a function of the number of total samples N_{total} in 2D. We consider the lattice sites $N_s = L_x \times L_y$ up to $N_s = 12 \times 10$. The statistical error is estimated by the blocking analysis and the bootstrap method with $N_{block} = 2^{10}$ and $N_{boot} = 2^{12}$. The error bar of σ_{S_2/N_s} is estimated for 32 independent simulations. The statistical error should satisfy $\sigma_{S_2/N_s} = \sqrt{c_{2D}(N_s)/N_{total}}$ with $c_{2D}(N_s)$ being a size-dependent constant. (b) Constant $c_{2D}(N_s)$ as a function of size N_s. We find that it satisfies $c_{2D}(N_s) \approx 2^{0.2N_s - 13}$ by fitting data for $N_s > 40$. As in the case of 1D, the prefactor (≈ 0.2) of N_s in 2D is much smaller than unity, suggesting that the computational cost is moderate although it is exponential in N_s.
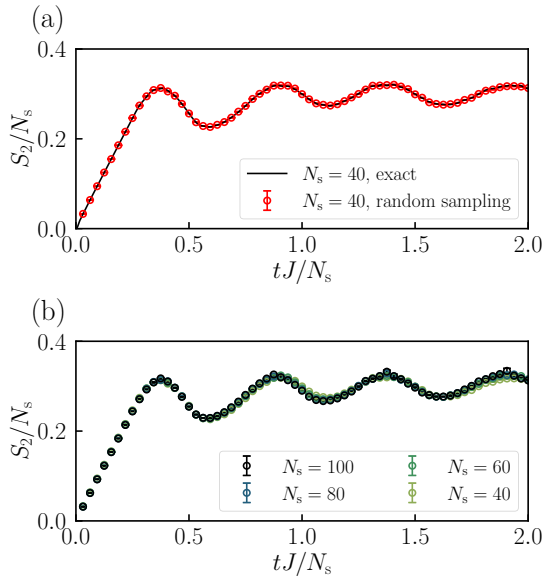

FIG. 6. (a) Comparison with the exact result of the time evolution of the Rényi entanglement entropy density in 1D for $N_s = 40$, which was the largest size obtained by the brute-force computation of the matrix permanent. The results are in good agreement. (b) Time evolution of the Rényi entanglement entropy density for much larger systems.
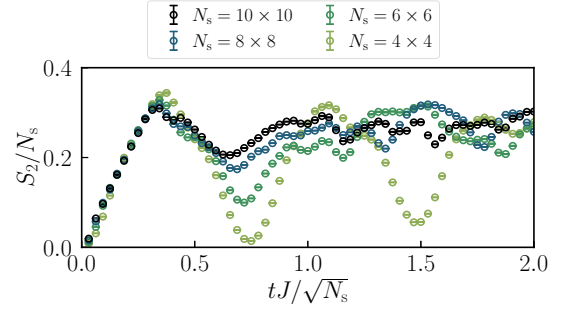

FIG. 7. Time evolution of the Rényi entanglement entropy density in 2D. We consider the lattice sites up to $N_s = 10 \times 10$ and calculate the Rényi entanglement entropy density when the system is divided into identical two parts.

We then study the larger systems up to $N_s = 100$. As shown in Fig. 6(b), the error bar is sufficiently small for all sizes that we study. The Rényi entanglement entropy densities for $N_s \geqslant 40$ nearly overlap, exhibiting the volume law scaling. Thus, the system size $N_s = 40$, corresponding to the largest size in our previous study, is large enough to capture the nature of the entanglement entropy density dynamics in the thermodynamic limit.

Next, we investigate the Rényi entanglement entropy density dynamics in a two-dimensional square lattices. As shown in Fig. 7, the Rényi entanglement entropy density grows linearly in time for a short time up to $tJ \approx 0.3\sqrt{N_s}$ for $N_s = L_x \times L_y$ with $L_x = L_y$. The behavior is consistent with the prediction from the previous studies on the entanglement entropy density dynamic in integrable systems with the Gaussian initial states [22,23], although our initial state is not the Gaussian state. The system-size dependence of the entanglement entropy density dynamics is rather small in this time regime. When the time is longer than $tJ \approx 0.3\sqrt{N_s}$, the entanglement entropy density shows a larger size dependence. It is difficult to extract the physically meaningful interpretation of the entanglement entropy density dynamics in the thermodynamic limit. However, as the system size increases, the fluctuation of the entanglement entropy density becomes smaller. The entanglement entropy density appears to converge to a certain value, exhibiting volume-law behavior of the entanglement entropy consistent with the previous studies [22,23]. Within the system sizes that we study, the entanglement entropy density approximately approaches the value close to ≈ 0.3 in both 1D and 2D.

IV. CONCLUSIONS AND OUTLOOK

In conclusion, we studied the dynamics of the Rényi entanglement entropy of insulating initial states in free boson systems. Owing to the non-Gaussian nature of the initial states, the calculation of the entanglement entropy required the evaluation of the matrix permanent, which has the exponential cost. We developed a random sampling method for evaluating the matrix permanent and found that the computational cost was reduced to $O(2^{\alpha N_s})$ with a small constant $\alpha \approx 0.2 \ll 1$ in one-dimensional and two-dimensional N_s-site systems at half filling. This reduction enabled us to study the

entanglement entropy dynamics for more than 100 sites in free boson systems.

Our results can be tested in experiments involving ultracold atoms in optical lattices and trapped ions. The dependence of entanglement entropy dynamics on system size is weak for one-dimensional systems with more than 40 sites; however, the dynamics have not converged even with 100 sites in 2D. Although performing sufficiently large-scale quantum simulations with current techniques remains challenging, it would be valuable to qualitatively verify the dependence of entanglement entropy dynamics on spatial dimensions. Our numerical data will assist in comparing these experimental results.

In the present study, we applied the simple random sampling method to the calculation of the Rényi entanglement entropy. One may consider more sophisticated sampling methods, such as the rejection sampling method [58–60] and the importance sampling method [61–63], to reduce the variance of the estimator for the matrix permanent. The upper and lower bounds of the entanglement entropy, i.e., the lower and upper bounds of the matrix permanent, would be utilized during such sophisticated sampling. As for the upper bound of the entanglement entropy, the second Rényi entanglement entropy is bounded above by the von Neumann entanglement entropy, and the von Neumann entanglement entropy is bounded above by the von Neumann entanglement entropy of a certain Gaussian state having the same two-point correlation functions as the original state [64,65]. The entanglement entropy of the Gaussian state can often be calculated efficiently. As for the lower bound of the entanglement entropy, by utilizing the following inequalities [55] for the matrix A in Eq. (14) that always fulfills $||A||_2 = 1$, with $|| \cdot ||_2$ being the operator 2-norm [33]:

$$\text{perm}A \leqslant \mathbb{E}\left[\prod_{i=1}^{n} \left| r_i^* \left(\sum_{j=1}^{n} a_{ij} r_j \right) \right| \right] = \mathbb{E}\left[\prod_{i=1}^{n} \left| \sum_{j=1}^{n} a_{ij} r_j \right| \right] \tag{43}$$

$$\leqslant \mathbb{E}\left[\left(\frac{1}{n} \sum_{i=1}^{n} \left| \sum_{j=1}^{n} a_{ij} r_j \right| \right)^n \right] \tag{44}$$

$$\leqslant \mathbb{E}\left[\left(\frac{1}{\sqrt{n}} \sqrt{\sum_{i=1}^{n} \left| \sum_{j=1}^{n} a_{ij} r_j \right|^2} \right)^n \right] \tag{45}$$

$$\leqslant \mathbb{E}[||A||_2] = 1, \tag{46}$$

one may consider the entanglement-entropy-like quantities

$$S_2' = -\ln \mathbb{E}\left[\prod_{i=1}^{n} \left| \sum_{j=1}^{n} a_{ij} r_j \right| \right], \tag{47}$$

$$S_2'' = -\ln \mathbb{E}\left[\left(\frac{1}{n} \sum_{i=1}^{n} \left| \sum_{j=1}^{n} a_{ij} r_j \right| \right)^n \right], \tag{48}$$

$$S_2''' = -\ln \mathbb{E}\left[\left(\frac{1}{\sqrt{n}} \sqrt{\sum_{i=1}^{n} \left| \sum_{j=1}^{n} a_{ij} r_j \right|^2} \right)^n \right], \tag{49}$$

satisfying

$$S_2 \geqslant S_2' \geqslant S_2'' \geqslant S_2''' \geqslant 0. \tag{50}$$

The quantities S_2', S_2'', and S_2''' can be calculated more efficiently than S_2 using the simple random sampling method or the importance sampling method because the quantities inside the expectation operator $\mathbb{E}$ are always nonnegative. When we wish to apply the rejection sampling method, for example, we may utilize the relation between the quantities $p(\boldsymbol{r}) = \prod_{i=1}^{n} r_i^* (\sum_{j=1}^{n} a_{ij} r_j)$ in Eq. (30) and $q(\boldsymbol{r}) := \prod_{i=1}^{n} |\sum_{j=1}^{n} a_{ij} r_j|$ that appears in Eq. (47). Since $q(\boldsymbol{r})$ is always nonnegative and the relation $p(\boldsymbol{r}) \leqslant q(\boldsymbol{r})$ holds for any $\boldsymbol{r}$, we can sample the random vector $\boldsymbol{r}$ from the distribution that generates $q(\boldsymbol{r})$ using the simple random sampling method and then sample $\tilde{s}$ from the uniform distribution on the interval $[0, q(\boldsymbol{r})]$. The sample $\boldsymbol{r}$ is accepted if $\tilde{s} \leqslant p(\boldsymbol{r})$ and is rejected otherwise. One can also combine the rejection and importance sampling methods [66]. The negative-sign-problem-like difficulty would be slightly alleviated when $p(\boldsymbol{r})$ is close to $q(\boldsymbol{r})$ for $\boldsymbol{r}$ that is likely to be sampled.

Although we specifically focused on the $010101 \cdots$-type CDW initial state, our approach can apply to other initial states that can be represented by a simple product of local Fock states. When using other initial states where the number of particles at each site is either 0 or 1, one has to appropriately modify the set G_{CDW} of charge rich sites in Eq. (3). When initial states have two or more particles at each site, the situation is more complex, although it is possible to extend the formalism using similar calculations. The random sampling method is also applicable to the dynamics of the entanglement entropy in general noninteracting Hamiltonians including long-range and random hopping terms. Such Hamiltonians only modify their eigenenergies and eigenstates defined in Eq. (6).

We expect that the computational cost of the random sampling method does not significantly depend on the details of the initial states for the parameter range that exhibits the volume-law scaling of the entanglement entropy. When the initial state contains N_b particles, we need to evaluate the permanent of an $N \times N$ matrix with $N = 2N_b$ to calculate the entanglement entropy. We speculate that the factor α in the computational cost $O(2^{\alpha N})$ of the random sampling method would be primarily determined by the size of the entanglement entropy per particle. This is because when the entanglement entropy per particle s is small and close to zero, the sample $\text{Re}\, p^{(m)}[\approx \exp(-sN)]$ in Eq. (30) should be close to unity for most samples m, indicating that the most of the samples are positive [see Fig. 2(a) as an example in the case of $s \approx 0$]. Consequently, the sampling efficiency increases and the factor α decreases, irrespective of the choice of the initial state as long as the entanglement entropy per particle is s.

As for the one-dimensional and two-dimensional systems that we study, the entanglement entropy per particle is $s \approx 2 \times 0.3$, whereas the corresponding factor is $\alpha \approx 0.2 \ll 1$. Our finding suggests that the factor α would be smaller than unity even when the entanglement entropy per particle is $O(1)$, which is the case in physically relevant systems exhibiting volume-law scaling of the entanglement entropy. This is in contrast to the conventional algorithms that always require the

summation of 2^N terms, corresponding to the case of $\alpha = 1$ in the random sampling method. It is intriguing to explore how the computational cost of the random sampling method depends on the entanglement entropy per particle in various initial states and in other noninteracting systems.

We specifically studied the dynamics of the Rényi entanglement entropy in free boson systems after a sudden quench. One may also consider the problems in the boson sampling devices [54,67]. There are several proposals for reducing the computational cost of the matrix permanent regarding the boson sampling procedure [68,69]. In practice, the feasible matrix size is up to $\approx 50 \times 50$ so far [70–72]. It is an interesting problem to study whether the sampling method also reduces the computational cost of the permanent of the matrix representing the boson sampling task.

As for the dynamics in the presence of interactions, namely, the dynamics in the Bose-Hubbard model, the information propagation and the particle transport would behave differently [73]. The former speed could be much faster than the latter speed. Since the numerical investigation of the entanglement entropy dynamics in strongly correlated systems is much more challenging, studying the dynamics in noninteracting boson systems using the random sampling method would help understand the information propagation in nonequilibrium quantum systems.

[1] M. Heyl, Rep. Prog. Phys. **81**, 054001 (2018).

[2] K. Życzkowski, P. Horodecki, M. Horodecki, and R. Horodecki, Phys. Rev. A **65**, 012101 (2001).

[3] M. A. Nielsen and I. L. Chuang, *Quantum Computation and Quantum Information* (Cambridge University Press, Cambridge, England, 2010).

[4] M. Greiner, O. Mandel, T. Esslinger, T. W. Hänsch, and I. Bloch, Nature (London) **415**, 39 (2002).

[5] P. Calabrese and J. Cardy, J. Stat. Mech. (2005) P04010.

[6] G. D. Chiara, S. Montangero, P. Calabrese, and R. Fazio, J. Stat. Mech. (2006) P03001.

[7] M. Cramer, C. M. Dawson, J. Eisert, and T. J. Osborne, Phys. Rev. Lett. **100**, 030602 (2008).

[8] M. Cramer, A. Flesch, I. P. McCulloch, U. Schollwöck, and J. Eisert, Phys. Rev. Lett. **101**, 063001 (2008).

[9] A. Flesch, M. Cramer, I. P. McCulloch, U. Schollwöck, and J. Eisert, Phys. Rev. A **78**, 033608 (2008).

[10] M. Fagotti and P. Calabrese, Phys. Rev. A **78**, 010306(R) (2008).

[11] A. M. Läuchli and C. Kollath, J. Stat. Mech. (2008) P05018.

[12] J. Eisert, M. Cramer, and M. B. Plenio, Rev. Mod. Phys. **82**, 277 (2010).

[13] P. Barmettler, D. Poletti, M. Cheneau, and C. Kollath, Phys. Rev. A **85**, 053625 (2012).

[14] J. H. Bardarson, F. Pollmann, and J. E. Moore, Phys. Rev. Lett. **109**, 017202 (2012).

[15] M. Cheneau, P. Barmettler, D. Poletti, M. Endres, P. Schauß, T. Fukuhara, C. Gross, I. Bloch, C. Kollath, and S. Kuhr, Nature (London) **481**, 484 (2012).

[16] S. Trotzky, Y.-A. Chen, A. Flesch, I. P. McCulloch, U. Schollwöck, J. Eisert, and I. Bloch, Nat. Phys. **8**, 325 (2012).

[17] G. Carleo, F. Becca, L. Sanchez-Palencia, S. Sorella, and M. Fabrizio, Phys. Rev. A **89**, 031602(R) (2014).

[18] A. Bauer, F. Dorfner, and F. Heidrich-Meisner, Phys. Rev. A **91**, 053628 (2015).

[19] I. Frérot and T. Roscilde, Phys. Rev. B **92**, 115129 (2015).

[20] I. Frérot and T. Roscilde, Phys. Rev. Lett. **116**, 190401 (2016).

[21] N. Laflorencie, Phys. Rep. **646**, 1 (2016).

[22] V. Alba and P. Calabrese, Proc. Natl. Acad. Sci. USA **114**, 7947 (2017).

[23] V. Alba and P. Calabrese, SciPost Phys. **4**, 017 (2018).

[24] S. Goto and I. Danshita, Phys. Rev. B **99**, 054307 (2019).

[25] K. Nagao, M. Kunimi, Y. Takasu, Y. Takahashi, and I. Danshita, Phys. Rev. A **99**, 023622 (2019).

[26] R. Yao and J. Zakrzewski, Phys. Rev. B **102**, 104203 (2020).

[27] Y. Takasu, T. Yagami, H. Asaka, Y. Fukushima, K. Nagao, S. Goto, I. Danshita, and Y. Takahashi, Sci. Adv. **6**, eaba9255 (2020).

[28] M. Kunimi and I. Danshita, Phys. Rev. A **104**, 043322 (2021).

[29] K. Nagao, Y. Takasu, Y. Takahashi, and I. Danshita, Phys. Rev. Res. **3**, 043091 (2021).

[30] R. Yoshii, S. Yamashika, and S. Tsuchiya, J. Phys. Soc. Jpn. **91**, 054601 (2022).

[31] C. Rylands, B. Bertini, and P. Calabrese, J. Stat. Mech. (2022) 103103.

[32] R. Kaneko and I. Danshita, Commun. Phys. **5**, 65 (2022).

[33] D. Kagamihara, R. Kaneko, S. Yamashika, K. Sugiyama, R. Yoshii, S. Tsuchiya, and I. Danshita, Phys. Rev. A **107**, 033305 (2023).

[34] S. Yamashika, D. Kagamihara, R. Yoshii, and S. Tsuchiya, Phys. Rev. Res. **5**, 043102 (2023).

[35] S. Yamashika, P. Calabrese, and F. Ares, arXiv:2410.14299.

[36] D. A. Abanin and E. Demler, Phys. Rev. Lett. **109**, 020504 (2012).

[37] A. J. Daley, H. Pichler, J. Schachenmayer, and P. Zoller, Phys. Rev. Lett. **109**, 020505 (2012).

[38] A. Elben, B. Vermersch, M. Dalmonte, J. I. Cirac, and P. Zoller, Phys. Rev. Lett. **120**, 050406 (2018).

[39] R. Islam, R. Ma, P. M. Preiss, M. Eric Tai, A. Lukin, M. Rispoli, and M. Greiner, Nature (London) **528**, 77 (2015).

[40] A. M. Kaufman, M. E. Tai, A. Lukin, M. Rispoli, R. Schittko, P. M. Preiss, and M. Greiner, Science **353**, 794 (2016).

[41] T. Brydges, A. Elben, P. Jurcevic, B. Vermersch, C. Maier, B. P. Lanyon, P. Zoller, R. Blatt, and C. F. Roos, Science **364**, 260 (2019).

[42] J. Watrous, Quantum computational complexity, in *Encyclopedia of Complexity and Systems Science*, edited by R. A. Meyers (Springer, New York, 2009), pp. 7174–7201.

[43] M. B. Hastings, I. González, A. B. Kallin, and R. G. Melko, Phys. Rev. Lett. **104**, 157201 (2010).

[44] J. Zhao, B.-B. Chen, Y.-C. Wang, Z. Yan, M. Cheng, and Z. Y. Meng, npj Quantum Mater. **7**, 69 (2022).

[45] H. J. Ryser, *Combinatorial Mathematics* (American Mathematical Society, Providence, RI, 1963), Vol. 14.

[46] R. A. Brualdi and H. J. Ryser, *Combinatorial Matrix Theory* (Cambridge University Press, Cambridge, England, 1991).

[47] D. G. Glynn, Eur. J. Comb. **31**, 1887 (2010).

[48] K. Balasubramanian, Combinatorics and diagonals of matrices, Ph.D. thesis, Indian Statistical Institute-Kolkata, 1980.

[49] E. Bax and J. Franklin, Technical Report No. CalTech-CS-TR-96-04, 1996.

[50] E. T. Bax, *Finite-Difference Algorithms for Counting Problems* (California Institute of Technology Pasadena, CA, 1998).

[51] D. G. Glynn, Des. Codes Cryptogr. **68**, 39 (2013).

[52] J. Huh, Phys. Rev. A **111**, 012418 (2025).

[53] L. Gurvits, in *Mathematical Foundations of Computer Science 2005*, edited by J. Jędrzejowicz and A. Szepietowski (Springer, Berlin, 2005), pp. 447–458.

[54] S. Aaronson and T. Hance, Quantum Inf. Comput. **14**, 541 (2014).

[55] R. Berkowitz and P. Devlin, Isr. J. Math. **224**, 437 (2018).

[56] V. Kocharovsky, V. Kocharovsky, and S. Tarasov, Entropy **22**, 322 (2020).

[57] E. Y. Loh, J. E. Gubernatis, R. T. Scalettar, S. R. White, D. J. Scalapino, and R. L. Sugar, Phys. Rev. B **41**, 9301 (1990).

[58] M. Huber and J. Law, in *Proceedings of the Nineteenth Annual ACM-SIAM Symposium on Discrete Algorithms*, SODA '08 (Society for Industrial and Applied Mathematics, Philadelphia, PA, 2008), pp. 681–689.

[59] J. Kuck, T. Dao, H. Rezatofighi, A. Sabharwal, and S. Ermon, in *Advances in Neural Information Processing Systems*, edited by H. Wallach, H. Larochelle, A. Beygelzimer, F. d'Alché-Buc, E. Fox, and R. Garnett (Curran, Red Hook, NY, 2019), Vol. 32.

[60] J. Harviainen, A. Röyskö, and M. Koivisto, in *Advances in Neural Information Processing Systems*, edited by M. Ranzato, A. Beygelzimer, Y. Dauphin, P. Liang, and J. W. Vaughan (Curran, Red Hook, NY, 2021), Vol. 34, pp. 213–224.

[61] M. Jerrum, A. Sinclair, and E. Vigoda, J. ACM **51**, 671 (2004).

[62] I. Bezáková, D. Štefankovič, V. V. Vazirani, and E. Vigoda, SIAM J. Comput. **37**, 1429 (2008).

[63] S. C. Kou and P. McCullagh, Biometrika **96**, 635 (2009).

[64] E. Bianchi, L. Hackl, and N. Yokomizo, J. High Energ. Phys. 03 (2018) 025.

[65] L. Hackl, E. Bianchi, R. Modak, and M. Rigol, Phys. Rev. A **97**, 032321 (2018).

[66] J. S. Liu, R. Chen, and W. H. Wong, J. Am. Stat. Assoc. **93**, 1022 (1998).

[67] S. Aaronson and A. Arkhipov, in *Proceedings of the Forty-Third Annual ACM Symposium on Theory of Computing* (ACM, New York, 2011), pp. 333–342.

[68] N. Quesada, R. S. Chadwick, B. A. Bell, J. M. Arrazola, T. Vincent, H. Qi, and R. García-Patrón, PRX Quantum **3**, 010306 (2022).

[69] P. Clifford and R. Clifford, Phys. Scr. **99**, 065121 (2024).

[70] A. Neville, C. Sparrow, R. Clifford, E. Johnston, P. M. Birchall, A. Montanaro, and A. Laing, Nat. Phys. **13**, 1153 (2017).

[71] J. Wu, Y. Liu, B. Zhang, X. Jin, Y. Wang, H. Wang, and X. Yang, Natl. Sci. Rev. **5**, 715 (2018).

[72] P.-H. Lundow and K. Markström, J. Comput. Phys. **455**, 110990 (2022).

[73] T. Kuwahara, T. V. Vu, and K. Saito, Nat. Commun. **15**, 2520 (2024).